Research Article Vol. 30, No. 4 / 14 Feb 2022 / Optics Express 4782
Optics EXPRESS

Pulsed-chaos MIMO radar based on a single flat-spectrum and Delta-like autocorrelation optical chaos source

WEIZHOU FENG,[1] NING JIANG,[1,*] YIQUN ZHANG,[1,2] JIAOYANG JIN,[1] ANKE ZHAO,[1] SHIQIN LIU,[1] AND KUN QIU[1]

[1]*School of Information and Communication Engineering, University of Electronic Science and Technology of China, 2006 Xiyuan Avenue, West High-Tech District, Chengdu 611731, China*
[2]*James Watt School of Engineering, University of Glasgow, Glasgow, UK*
[*]*uestc_nj@uestc.edu.cn*

Abstract: We propose and demonstrate a pulsed-chaos multiple-input-multiple-output (MIMO) radar system in this paper. In the proposed MIMO radar system, multi-channel pulsed chaotic signals are extracted from an optical seed chaos source with Delta-like autocorrelation and flat spectrum. The seed chaos source is generated by passing the chaotic output of an external-cavity semiconductor laser through a dispersive self-feedback phase-modulation loop and used for MIMO radar signal generation. The cross-correlation characteristics of MIMO radar signals, the maximum channel number of separable mixed echoes, as well as the performances of multi-target ranging and anti-interference in the proposed pulsed-chaos MIMO radar system are systematically investigated. The results indicate that multi-channel pulsed-chaos signals with Delta-like autocorrelation can be simultaneously generated from the seed chaos source, and excellent quasi-orthogonality of transmission radar signals can be guaranteed. Moreover, it is demonstrated that the proposed pulsed-chaos MIMO radar supports multi-target ranging with a centimeter-level resolution and can maintain satisfactory performance under low SNR scenarios with various interferences.

1. Introduction

Multiple-input-multiple-output (MIMO) radar has shown great advantages in high-resolution imaging, target detection and tracking, as well as parameter estimation in recent years [1–4]. The key of MIMO radar is to employ multiple antennas for emitting orthogonal waveforms and simultaneously use multiple antennas for receiving the echoes reflected by the targets to achieve waveform diversity [5]. Compared with the phased-array radar that only transmits narrow beam, the MIMO radar can transmit both narrow beam and wide beam, as such has higher controllable degrees of freedom [6]. Since the transmitted signals of antennas are uncorrelated orthogonal waveforms, the MIMO radar is capable to separate the individual transmission signals from the received mixture echo waveforms, thereby the number of observation channels and degrees of freedom in the MIMO radar is much more than the number of transceiver antennas. For this reason, the antenna aperture of the receiver array can be enlarged, and a large-aperture equivalent array can be obtained. Therefore, the MIMO radar shows a higher spatial resolution with respect to the real aperture radar.

Since the orthogonality of transmitted waveforms is critical to separate and process the radar multi-echo signals, the orthogonal waveform design is one of the most important factors for a MIMO radar. To obtain more prominent radar performance, several types of orthogonal waveform design methods for MIMO radar have been proposed in recent years. P. Stoica et al., proposed a scheme by designing a covariance matrix of the detection signal vector to maximize the power around the target location of interest [7]. Based on some prior knowledge of the target

#450949 https://doi.org/10.1364/OE.450949
Journal © 2022 Received 9 Dec 2021; revised 9 Jan 2022; accepted 11 Jan 2022; published 31 Jan 2022

Optics EXPRESS

response, Y. Yang and colleagues designed a MIMO radar waveform diversity scheme to estimate the extended targets [8]. Regarding the MIMO radars without the prior knowledge, S. Sen and Y. Chen proposed the waveform design method based on mutual information [9,10]. Moreover, C. Y. Chen et al. proposed a waveform design method based on frequency hopping [11], and W. Q. Wang proposed an OFDM chirp waveform diversity scheme using random matrix modulation [12]. In addition, quadrature phase encoding waveforms and quadrature frequency encoding waveforms have also been designed for implementing MIMO radars, in virtue of the optimization algorithm, the genetic algorithm, as well as the simulated annealing and neighborhood search algorithms [13–15].

Chaos waveforms generated from nonlinear dynamical systems are aperiodic, sensitive to initial values, and have low cross-correlation peaks and low autocorrelation side-lobes. Based on these features, chaos-based radars attracted a lot of attention recently. Up to the present, most of the attention is focused on the digital chaos-based radar [16,17], since the generation of digital chaos does not require complex algorithm optimization, and waveforms of any length can be generated through simple iterations. Nevertheless, due to the electronic bottleneck, the bandwidth of transmission signal of the digital chaos-based radar is relatively low in practice. While the spatial resolution of radar is intrinsically determined by the effective bandwidth of the transmission signal [18], as such the feasibility of the implementation of high-resolution digital chaos-based radar is limited.

To improve the resolution and precision performances of chaos-based radar, using optical chaotic signal generated by semiconductor laser (SL) as radar waveforms has been proposed [19–33]. Under such a scenario, high resolution ranging or imaging can be achieved with one single chaotic channel. Recently, generation of uncorrelated multi-channel chaos for MIMO radar through electrical heterodyning a single-channel seed chaos has been reported in [33], wherein a series of multiple uncorrelated signals are simultaneously generated from a typical optical chaos source, namely an external-cavity semiconductor laser (ECSL) subject to conventional optical feedback. It paves a novel way to implement MIMO radar with features of high resolution and precision, anti-interference, as well as low probability of interception. While some crucial issues, such as novel easily-implemented waveform design and generation of huge number of orthogonal MIMO radar signals with single optical chaos source, the performances of ranging, tracking and anti-interference, as well as the feasibility of applications in the fields of multi-target detection, imaging etc., deserve thorough discussions. This motivates further investigations in the field of MIMO radar in virtue of the features of wideband and noise-like waveforms of ECSL-based optical chaos.

In the conventional ECSL-based chaos sources, due to the feedback light being a delayed linear replica of the output of semiconductor laser, an obvious time delay signature (TDS) exists in the autocorrelation function (ACF) trace of conventional ECSL-outputted chaos [34,35]. This property would induce false side-lobes in the trace of cross-correlation function (CCF) of the reference signal and echo signal, and then cause ranging ambiguity. On the other hand, the spectrum of conventional ECSL-based chaos is concentrated nearby the relaxation oscillation frequency (f_{RO}). Under such scenario, with bandwidth-limited photodetector (PD) and analog-to-digital converter (ADC), the energy of the low-frequency band (0Hz~f_{RO}) radar signal is small, this would result in low energy-utilization efficiency for radar application. Therefore, it is valuable to improve the flatness of spectrum and simultaneously suppress the TDS of ECSL-based chaos to obtain Delta-like autocorrelation, as well as explore novel multi-channel orthogonal chaos waveform design methods for MIMO radar.

In this paper, we propose and demonstrate a pulsed-chaos MIMO radar system using a flat-spectrum wideband optical chaos source with Delta-like autocorrelation. A novel chaos source originated from a conventional ECSL cascaded by a dispersive self-feedback phase-modulated loop (SFPML) is experimentally established and used for multiple quasi-orthogonal pulsed-chaos

Optics EXPRESS

waveform generation. The feasibility and performance of the pulsed-chaos MIMO radar are systematically discussed.

2. System configuration and principle

Figure 1 presents the schematic of the proposed pulsed-chaos MIMO radar system. This system mainly comprises a multi-channel pulsed-chaos source module, as well as a transceiver and processing module. In the multi-channel pulsed-chaos source module, a seed chaos signal is first generated by passing the initial chaos outputted from a conventional ECSL through a dispersive self-feedback phase modulation loop. Then, the seed chaos signal is split into n paths by an optical beam splitter (OBS). On each path, the chaotic signal is delayed by an optical delay line (DL) and then converted into an electrical signal by a PD. The delay times of DLs are set as different to obtain time-domain non-overlapped signals for different channels. Subsequently, the continuous chaotic signals on the n paths are synchronously pulsed by electronic switches that are controlled by a common clock, and consequently, a series of pulsed-chaos waveforms are obtained on each path. The pulse repetition frequency and duty cycle are determined by the "on" and "off" durations of the switch in each cycle. In the transceiver and processing module, there are n sets of transceiver and processing submodules (dashed boxes) for the n channels. In each submodule, the corresponding pulsed-chaos signal is firstly filtered as a band-limited signal through a low-pass filter (LPF), and then divided into two parts by a power splitter (PS). One is first mixed with a local oscillator (LO), then amplified by a radio-frequency amplifier (Amp), and finally sent into the free space by the transmitting antenna (T). While the other part is sent into a local signal processing module and used as the reference signal for target detection. On the other hand, the hybrid echoes received by receiver antenna (R) are demodulated by the same LO and then sent into the signal processing module. The local signal processing module is adopted to detect the time delay information of each channel by calculating the cross-correlation between the reference signal and the demodulated echo, and it can be realized by a field programmable gate array (FPGA) or a personal computer. It is worth mentioning that the LO and the signal processing module for all channels can be shared.

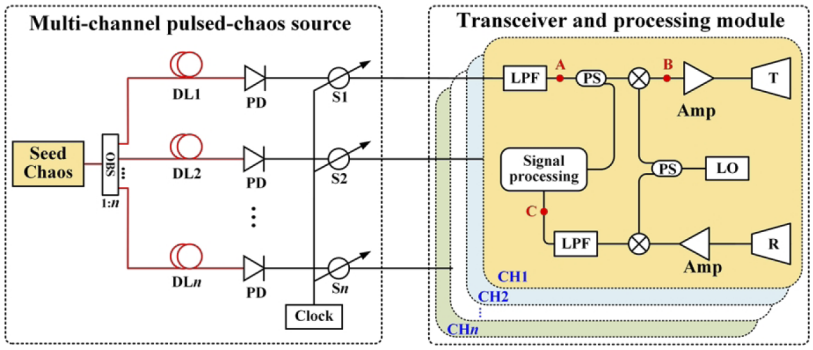

Fig. 1. Schematic of pulsed chaos MIMO radar system. OBS, optical beam splitter; DLs, delay lines; S, switch; PD, photodetector; Amp, radio-frequency amplifier; LPF, low-pass filter; PS, power splitter; LO, local oscillator; T, transmitter antenna; R, receiver antenna.

Figure 2 shows the experimental setup of the seed chaos source in the proposed MIMO radar system. It is composed of a conventional ECSL that generates an initial chaos signal and a SFPML that consists of phase modulator (PM), dispersive element (D), PD, variable optical attenuator (VOA), and RF amplifier (Amp). By passing the initial chaotic signals through the self-feedback-driving phase modulator and dispersive component, a flat-spectrum and TDS-suppressed seed chaos can be obtained. Compared with the initial chaotic signal, the spectrum

Optics EXPRESS

flatness and bandwidth of the seed chaos can be significantly enhanced, and simultaneously, the TDS of the initial chaos can be eliminated and a Delta-like autocorrelation is obtained. In our experiment, the bias current for DFB laser is 16.5 mA which is 1.5 times the threshold current (11 mA), the operation wavelength of DFB laser is set as 1551.33 nm, the time delays of the ECSL feedback loop and the SFPML are $\tau_1 = 100.2$ ns and $\tau_2 = 24.34$ μs, respectively. Under these conditions, the relaxation oscillation frequency of the DFB laser is 4.27 GHz, and the effective bandwidth of the initial chaos is about 5.82 GHz. Here the effective bandwidth is defined as that in [36,37]. A dispersion compensation fiber with a dispersion coefficient of 638 ps/nm is employed as the dispersive component. The bandwidth of the phase modulator is 20GHz, and the half-wave voltage is 3.8 V. The PM modulation depth is about 2.3. The maximum power gain of the RF amplifier is 38 dB with a bandwidth of 18 GHz. A 20 GS/s real-time digital oscilloscope is used to measure and record the relevant electrical signals. On the basis of the experimentally-generated seed chaos, the investigations on the performance of the pulsed-chaos MIMO radar are carried out by numerical simulations. In the simulation, the sampling rate of ADCs is set as 20GS/s, two identical equal-ripple finite impulse response (FIR) low-pass filters with 3dB passband of 2.2GHz are adopted to match the operation frequency bandwidths of the antennas and suppress the noise at the transceivers, the frequency of the local oscillators is set as 5GHz, the operation frequency ranges of the transceiver amplifiers and antennas are from 1GHz to 9GHz, the pulse repetition frequency of pulsed-chaos signal extraction is 20 kHz, and the duty cycle is 0.02.

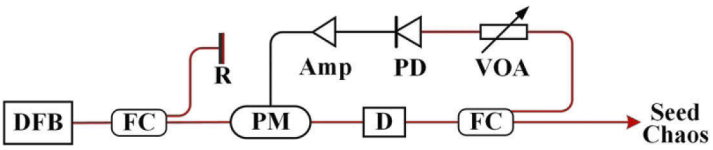

Fig. 2. Experimental setup of seed chaos source. DFB, distributed-feedback semiconductor laser; R, reflector; PM, phase modulator; D, dispersive compensation fiber; FC, fiber coupler; VOA, variable optical attenuator; PD, photodetector; Amp, radio-frequency amplifier.

Figure 3 shows the schematic of the multi-channel pulsed-chaos signal extraction from seed chaos, in virtue of the optical delay segmentation (ODS). Assuming that the number of channels is n, the number of pulses per channel is m, and the delay of the *i-th* path is $(i-1)T$ (with respect to that of Channel 1), where T is the delay difference between the delay lines of adjacent channels, which can be considered as the delay time step here. The initial states of the switches are off. In each cycle of the pulsed-chaos extraction, the switch conduction time is T_0 (pulse width), and the off-time is T_r. The duty cycle of the pulsed-chaos signal is determined by $\eta = T_0/(T_0 + T_r)$ and the pulsing repetition frequency is determined by $1/(T_0 + T_r)$. The switches are turned on for the first time at T_{s1}. To guarantee the multi-channel pulsed-chaos signals are quasi-orthogonal (uncorrelated), it is necessary to keep the pulses of each segmentation are not overlapped in time domain, as such the following conditions should be satisfied,

$$\begin{cases} T_{s1} \geq (n-1)T \\ T_0 \leq T \end{cases} \tag{1}$$

In the following simulations, unless otherwise stated, the values of T and T_0 are fixed at 1 μs.

Optics EXPRESS

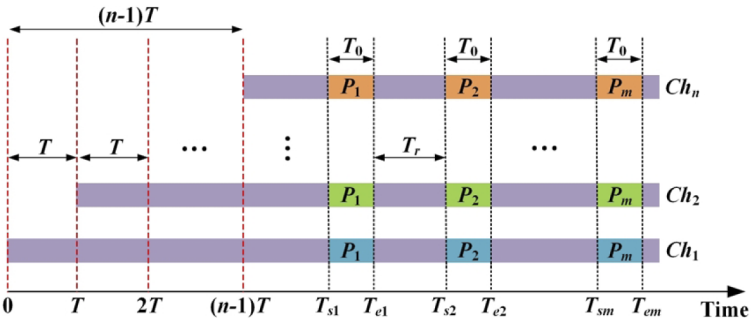

Fig. 3. Schematic of multi-channel uncorrelated pulsed-chaos signal generation, in virtue of optical delay segmentation

3. Results and analysis

3.1. Characteristics of radar signals

Figure 4 presents the temporal waveforms, power spectrum and ACF traces, for the seed chaos, the pulsed-chaos signal (position A in Fig. 1), the transmission radar signal (position B in Fig. 1) and the back-to-back echo signal (position C in Fig. 1) for Channel 1, respectively. Here the back-to-back echo signal is obtained by directly demodulating the transmission radar signal with a LO signal and then filtering the demodulated signal with a LPF. The parameters of the LO and LPF are identical to those for transmission signal generation. It is demonstrated that the temporal waveform of the seed chaos shows irregular rapid oscillations, and its power spectrum is flat in the range of 0 to 10 GHz (Figs. 4(a1)-(a2)), which enables the proposed MIMO radar to have a low probability of interception and high energy-utilization efficiency. Moreover, both of the TDSs (τ_1 and τ_2) for the ECSL and SFPML are completely suppressed in the ACF trace (Figs. 4(a3)). To match the operation frequency bandwidth of the transmission antenna, the pulsed-chaos signal is filtered by a LPF, with which the bandwidth of the baseband pulsed-chaos signal is concentrated in 0–3 GHz (Figs. 4(b1) and (b2)). Besides, the pulsed-chaos signal maintains excellent Delta-like autocorrelation characteristic, as that shown in Fig. 4(b3). The transmission radar signal is generated by modulating the filtered pulsed-chaos signal with a 5 GHz sinusoidal signal generated by a LO. As shown in Fig. 4(c2), the power spectrum of the transmission radar signal is symmetric at 5 GHz, and the bandwidth is doubled with respect to that of the baseband pulsed-chaos signal. Moreover, the ACF trace in Fig. 4(c3) shows that although the pulsed-chaos signal is modulated by a sinusoidal signal, Delta-like autocorrelation can also be maintained. Regarding the back-to-back echo signal, as shown in Figs. 4(d1)–4(d3), its temporal waveform, RF spectrum and ACF features are much similar to the filtered baseband pulsed-chaos signal that plays the role of reference signal for radar detection. Since the echo signal is demodulated with a LO and then filtered by a low-pass filter with a 3 dB passband of 2.2 GHz, as such the frequency components higher than 2.2 GHz are significantly suppressed, and the power spectrum in the region higher than 4 GHz is almost constant, as that shown in Fig. 4(d2). In addition, it is worth mentioning that the corresponding results for other channels are similar, but not shown here for the sake of simplicity.

3.2. Cross-correlation analysis

Figure 5(a) shows the cross-correlation (non-diagonal) and autocorrelation (diagonal) of the multi-channel transmission signals. Here 10 channels are taken into consideration for instance, and the correlation length (the time length of the signal segment used for cross-correlation or autocorrelation calculation) is fixed at 5μs. The results show that the cross-correlation between

Optics EXPRESS

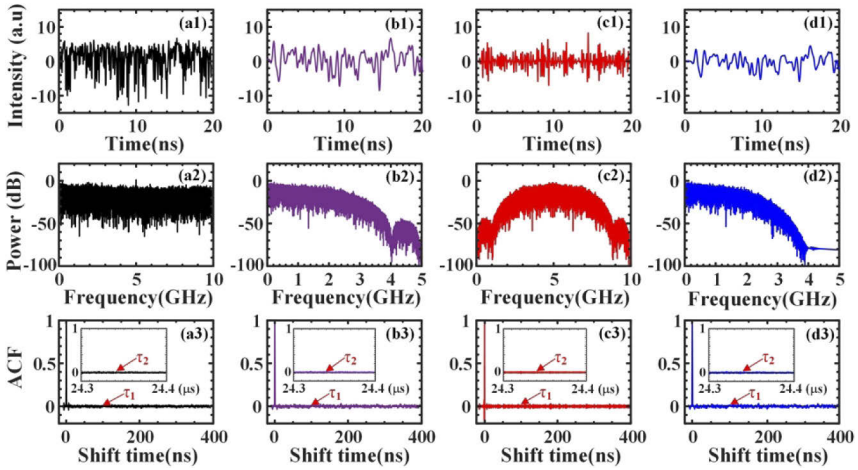

Fig. 4. Temporal intensity waveforms (first row), power spectrum (second row) and ACF (third row) of the seed chaos (first column), the pulsed-chaos signal (second column), the transmission radar signal (third column), and the back-to-back echo signal (fourth column)

any pairwise channels is maintained at a very low level close to 0. That is, in the proposed pulsed-chaos MIMO radar system, excellent quasi-orthogonality of transmission radar signals can be guaranteed. In addition, our repeating simulations demonstrate that the longer the correlation length, the closer the cross-correlation between pairwise-channels signals to 0. On the other hand, when the delay time T is smaller than T_0, the pulsed-chaos signals would be overlapped to some extent, and then the orthogonality of the MIMO radar signals would be degraded. Therefore, it is valuable to discuss the influence of the overlapping induced by improper segmentation on the cross-correlation of MIMO radar signals. Figure 5(b) shows the variation of the average cross-correlation coefficient (CC) of pairwise-channels signals versus the overlap ratio. Here, the overlap ratio is defined as $1\text{-}T/T_0$. It is indicated that as the increase of the overlap ratio, the average CC value increases gradually. Nevertheless, as long as the overlap ratio is smaller than 0.2, the average CC can be maintained at a level smaller than 0.1. Therefore, it can be concluded that the proposed pulsed-chaos MIMO radar system is robust to some overlap induced by imperfect segmentation.

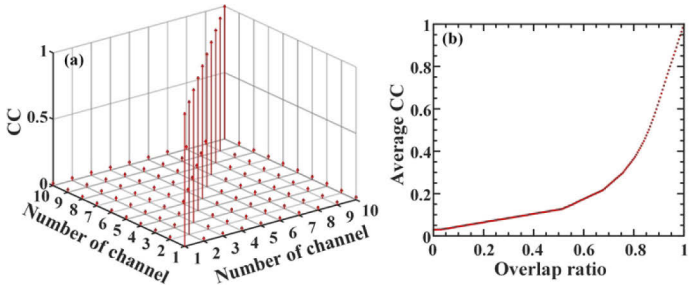

Fig. 5. (a) Correlation of multi-channel transmission signals, and (b) average cross-correlation coefficient versus overlap ratio in an exemplary 10-channel MIMO radar system.

Optics EXPRESS

3.3. Maximum number of channels

In MIMO radar systems, the received signal is a superposition of multiple signals. Under such a case, the channel cross-interference would degrade the performance of MIMO system, as such the maximum number of channels that supports separable echo signals in MIMO radar system is limited. In this subsection, we discuss the maximum number of channels that the proposed pulsed-chaos MIMO radar system supports. To quantitatively evaluate the performance of the proposed MIMO radar system, the peak-sidelobe level (PSL) that is defined as the ratio of the maximum sidelobe to the peak in the CCF trace of the reference signal and echo signal [19], as well as the peak-to-standard deviation of sidelobe level (PSL_{std}) that is defined as the ratio between the CCF peak and three times the standard deviation of the noise floor in the CCF trace [32], are calculated. Generally, a radar system can maintain a satisfactory ranging performance when the PSL is lower than −3dB [19], and provide a ranging accuracy error in the order of centimeter when the PSL_{std} is higher than 6dB [32]. For this reason, these two parameters are used as the reference thresholds to evaluate the maximum number of channels.

Figure 6 presents the influence of the channel number on the performance of the proposed MIMO radar system working in the back-to-back scenario identical to that in Fig. 4(d1)-(d3). Here two cases with different correlation lengths are discussed. It is demonstrated that although the correlation lengths are different in Figs. 6(a) and 6(b), the variation trends of PSL and PSL_{std} traces are respectively similar. Specifically, as the number of channels increases, the PSL of the proposed pulsed-chaos MIMO radar system increases gradually, while the corresponding PSL_{std} decreases. These phenomena are because of that the channel cross-interference plays the role of noise, and the more the channels of MIMO radar system, the more serious the influence of noise, consequently, the higher the PSL and the lower the PSL_{std}. Moreover, it is indicated that a longer correlation length can support a larger channel number. When the correlation length is 0.5μs, the maximum channel number supporting a centimeter precision is about 50, while with a correlation length of 1μs, the maximum channel number can be further enhanced to larger than 80.

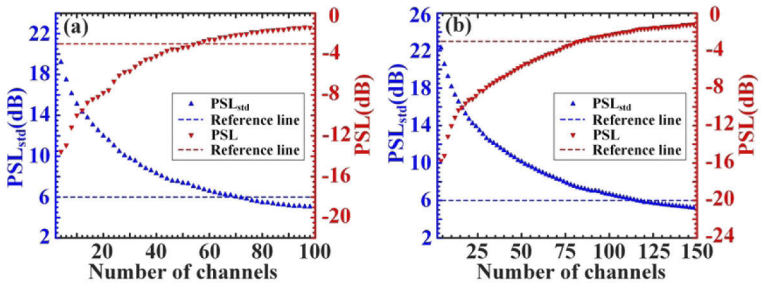

Fig. 6. Performance of the proposed pulsed-chaos MIMO radar versus the number of channels, in the cases with correlation lengths of (a) 0.5μs and (b) 1μs.

To further investigate the influences of channel number and correlation length on the performance of the proposed MIMO radar system, we present in the space of channel number and correlation length in Fig. 7. The results indicated the variations of PSL and PSL_{std} in the space of channel number and correlation length. The results indicate that, for a fixed channel number, with the selection of a long enough correlation length, satisfactory performance with a PSL lower than −3 dB and a PSL_{std} higher than 6 dB can be easily achieved in the proposed pulsed-chaos MIMO system. Moreover, the longer the correlation length, the better the performance of MIMO radar system, and the larger the maximum number of channels. Nevertheless, in practice, since longer correlation length requires longer calculation time, this would degrade the real-time performance of radar detection, as such there is a trade-off between the maximum number of channel and the real-time performance.

Optics EXPRESS

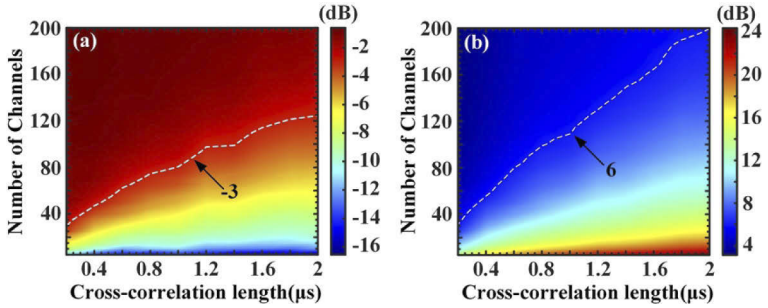

Fig. 7. Influence of correlation length and channel number on (a) PSL and (b) PSL_{std}.

3.4. Multi-target ranging

In this subsection, we explore the multi-target ranging performance of the proposed pulsed-chaos MIMO radar system. Figure 8 demonstrate the ranging results for three targets away from 13.2m, 13.5m, and 15m, by calculating the peak positions in CCF trace of the reference signal and the demodulated echo signal. Here, for the sake of simplicity, the transmission loss is ignored and only the results on Channel 1 are presented. It is indicated that all the three targets can be simultaneously detected, and the similar CCF peaks are observed. By measuring the full-width at half-maximums (FWHM) of the CCF peaks, the ranging resolution is about 5cm, which is in line with the theoretical estimation results $D = c/2B$, where D stands for the range resolution, c stands for the light velocity in free space, and B denotes the bandwidth of reference signal. Repeating simulation results for other channels and different target positions are similar. Therefore, the proposed pulsed-chaos MIMO radar can support a target resolution of 5cm. The range resolution can be further improved by expanding the bandwidth of the baseband pulsed-chaos signal.

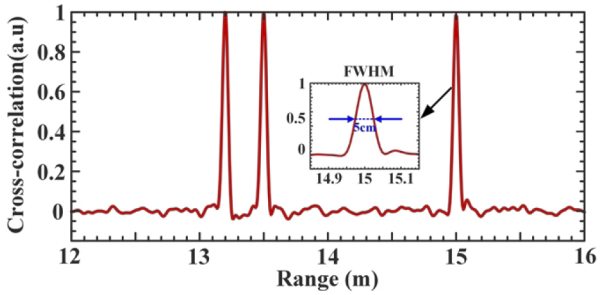

Fig. 8. Cross-correlation trace of multi-target ranging in the case with three targets away from 13.2 m, 13.5 m, and 15 m, respectively. The inset shows the FWHM of the CCF peak at 15 m.

3.5. Anti-interference performance

In practice, the performance of radar system is inevitably affected by various interferences. In general, the typical interferences for a MIMO radar system include the Gaussian white noise interference, the sine wave interference, the pulse interference, as well as the cross-interference induced by the MIMO radar itself. Figure 9 presents the influence of these typical interferences on the PSL and PSL_{std} in the proposed MIMO radar system. Here SNR is the ratio of transmitted signal power to interference power, and the frequencies of sine-wave interference and pulse interference are set as 2.4 GHz and 2 GHz respectively, while the cross-interference induced by

Optics EXPRESS

the MIMO channels are originated from the same chaos source as that shown in Fig. 1. The gray and light-blue horizontal lines denote the reference lines that stand for the ideal case with no interference. The results indicate that, these 4 typical interferences show similar influences on the PSL and PSL_{std}. As the increase of SNR, the performance gradually gets better and better. When the SNR is 10 dB, the performance is approximately identical to that of the ideal case (with no interference). On the other hand, it is demonstrated that the proposed pulsed-chaos MIMO radar can guarantee a satisfactory performance (PSL<-3 dB, $PSL_{std} > 6$ dB) even when the SNR is as low as -24 dB, which means the proposed pulsed-chaos MIMO radar shows excellent anti-interference capability. This is in line with the anti-interference analysis results in [20].

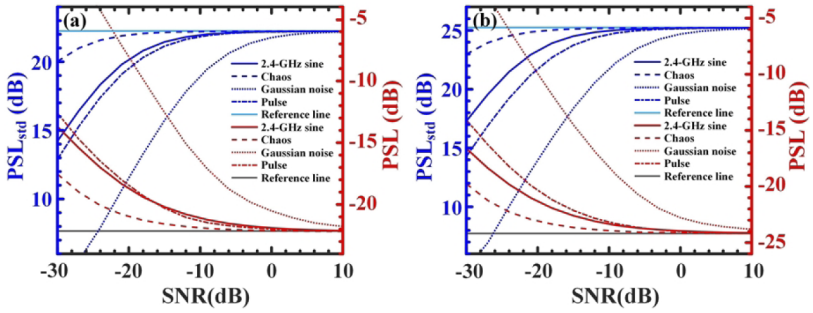

Fig. 9. Anti-interference performance of the proposed pulsed-chaos MIMO radar versus SNR, in the cases with correlation lengths of (a) 0.5μs and (b) 1μs.

4. Conclusion

In this work, we propose a pulsed-chaos MIMO radar system, by extracting multi-channel pulsed-chaos signals from a common optical seed chaos source with flat-spectrum and Delta-like autocorrelation. The seed chaos is experimentally generated by passing the conventional ECSL-generated chaotic signal through a dispersive SFPML. Based on the experimental seed chaos source, the cross-correlation characteristics of MIMO transmission signals, the maximum channel number of separable mixed echoes, the multi-target detection performance, as well as the anti-public interference performance of the pulsed-chaos MIMO radar system are systematically investigated. The results demonstrate that, the baseband pulsed-chaos signals show excellent Delta-like autocorrelation feature, and the cross-correlation of transmission radar signals is close to 0, which guarantees the quasi-orthogonality of MIMO radar signals. Several tens of MIMO channels with satisfactory performance can be supported in the proposed pulsed-chaos radar system, and multi-target ranging with a resolution of 5cm can be achieved. Moreover, the proposed MIMO radar system is robust to the sinusoidal interference, Gaussian white noise interference, pulse interference and channel cross-interference. Even in the case of a SNR smaller than -20dB, satisfactory performance can be guaranteed. This work paves a way for implementing MIMO radar in virtue of wideband optical chaos source.

Funding. National Natural Science Foundation of China (61671119, 62171087); Sichuan Science and Technology Program (2021JDJQ0023); Fundamental Research Funds for the Central Universities (ZYGX2019J003); Science and Technology Commission of Shanghai Municipality (SKLSFO2020-05).

Disclosures. The authors declare no conflicts of interest.

Data availability. The data used to support the findings of this study are available from the corresponding author upon request.

Optics EXPRESS

References

1. S. S. Guo, G. L. Cui, L. J. Kong, Y. L. Song, and X. B. Yang, "Multipath analysis and exploitation for MIMO through-the-wall imaging radar," IEEE J. Sel. Top. Appl. Earth Observations Remote Sensing **11**(10), 3721–3731 (2018).
2. H. Q. Li, G. L. Cui, L. J. Kong, G. H. Chen, M. Y. Wang, and S. S. Guo, "Robust human targets tracking for MIMO through-wall radar via multi-algorithm fusion," IEEE J. Sel. Top. Appl. Earth Observations Remote Sensing **12**(4), 1154–1164 (2019).
3. X. X. Yu, G. L. Cui, J. Yang, and L. J. Kong, "MIMO radar transmit–receive design for moving target detection in signal-dependent clutter," IEEE Trans. Veh. Technol. **69**(1), 522–536 (2020).
4. J. X. Lu, F. F. Liu, J. Y. Sun, Q. H. Liu, and Y. J. Miao, "Joint estimation of Target Parameters and System Deviations in MIMO Radar with Widely Separated Antennas on Moving Platforms," IEEE Trans. Aerosp. Electron. Syst. **57**(5), 3015–3028 (2021).
5. I. Bekkerman and J. Tabrikian, "Target detection and localization using MIMO radars and sonars," IEEE Trans. Signal Process. **54**(10), 3873–3883 (2006).
6. A. Hassanien and S. A. Vorobyov, "Phased-MIMO radar: A tradeoff between phased-array and MIMO radars," IEEE Trans. Signal Process. **58**(6), 3137–3151 (2010).
7. P. Stoica, J. Li, and Y. Xie, "On probing signal design for MIMO radar," IEEE Trans. Signal Process. **55**(8), 4151–4161 (2007).
8. Y. Yang and R. S. Blum, "MIMO radar waveform design based on mutual information and minimum mean-square error estimation," IEEE Trans. Aerosp. Electron. Syst. **43**(1), 330–343 (2007).
9. S. Sen and A. Nehorai, "OFDM MIMO radar with mutual-information waveform design for low-grazing angle tracking," IEEE Trans. Signal Process. **58**(6), 3152–3162 (2010).
10. Y. Chen, Y. Nijsure, C. Yuen, Y. H. Chew, Z. Ding, and S. Boussakta, "Adaptive distributed MIMO radar waveform optimization based on mutual information," IEEE Trans. Aerosp. Electron. Syst. **49**(2), 1374–1385 (2013).
11. C. Y. Chen and P. P. Vaidyanathan, "MIMO radar ambiguity properties and optimization using frequency-hopping waveforms," IEEE Trans. Signal Process. **56**(12), 5926–5936 (2008).
12. W. Q. Wang, "MIMO SAR OFDM chirp waveform diversity design with random matrix modulation," IEEE Trans. Geosci. Remote Sensing **53**(3), 1615–1625 (2015).
13. H. Deng, "Polyphase code design for orthogonal netted radar systems," IEEE Trans. Signal Process. **52**(11), 3126–3135 (2004).
14. H. Deng, "Discrete frequency-coding waveform design for netted radar systems," IEEE Signal Processing Letters **11**(2), 179–182 (2004).
15. B. Liu, "Orthogonal discrete frequency-coding waveform set design with minimized autocorrelation sidelobes," IEEE Trans. Aerosp. Electron. Syst. **45**(4), 1650–1657 (2009).
16. Y. Jin, H. Wang, W. Jiang, and Z. Zhuang, "Complementary-based chaotic phase-coded waveforms design for MIMO radar," IET Radar, Sonar & Navigation **7**(4), 371–382 (2013).
17. S. Hong, F. Zhou, Y. Dong, Z. Zhao, Y. Wang, and M. Yan, "Chaotic phase-coded waveforms with space-time complementary coding for MIMO radar applications," IEEE Access **6**, 42066–42083 (2018).
18. G. S. Antonio, D. R. Fuhrmann, and F. C. Robey, "MIMO Radar Ambiguity Functions," IEEE Journal of Selected Topics in Signal Processing **1**(1), 167–177 (2007).
19. F. Y. Lin and J. M. Liu, "Chaotic lidar," IEEE J. Sel. Top. Quantum Electron. **10**(5), 991–997 (2004).
20. F. Y. Lin and J. M. Liu, "Chaotic radar using nonlinear laser dynamics," IEEE J. Quantum Electron. **40**(6), 815–820 (2004).
21. F. Y. Lin and J. M. Liu, "Ambiguity functions of laser-based chaotic radar," IEEE J. Sel. Top. Quantum Electron. **40**(12), 1732–1738 (2004).
22. B. J. Wang, Y. C. Wang, L. Q. Kong, and A. B. Wang, "Multi-target real-time ranging with chaotic laser radar," Chin. Opt. Lett. **6**(11), 868–870 (2008).
23. B. J. Wang, T. Zhao, and H. K. Wang, "Improvement of signal-to-noise ratio in chaotic laser radar based on algorithm implementation," Chin. Opt. Lett. **10**(5), 052801 (2012).
24. M. J. Zhang, Y. N. Ji, Y. N. Zhang, Y. Wu, H. Xu, and W. P. Xu, "Remote radar based on chaos generation and radio over fiber," IEEE Photonics J. **6**(5), 1–12 (2014).
25. B. J. Wang, H. Xu, P. Yang, L. Liu, and J. X. Li, "Target detection and ranging through lossy media using chaotic radar," Entropy **17**(4), 2082–2093 (2015).
26. H. Xu, B. J. Wang, H. Han, L. Liu, J. X. Li, Y. C. Wang, and A. B. Wang, "Remote imaging radar with ultra-wideband chaotic signals over fiber links," Int. J. Bifurcation Chaos **25**(11), 1530029 (2015).
27. D. Z. Zhong, G. L. Xu, W. Luo, and Z. Z. Xiao, "Real-time multi-target ranging based on chaotic polarization laser radars in the drive-response VCSELs," Opt. Express **25**(18), 21684–21704 (2017).
28. C. H. Cheng, C. Y. Chen, J. D. Chen, D. K. Pan, K. T. Ting, and F. Y. Lin, "3D pulsed chaos lidar system," Opt. Express **26**(9), 12230–12241 (2018).
29. D. Z. Zhong, Z. Z. Xiao, G. Z. Yang, N. Zhen, and H. Yang, "Real-time ranging of the six orientational targets by using chaotic polarization radars in the three-node VCSEL network," Opt. Express **27**(7), 9857–9867 (2019).

Optics EXPRESS

30. H. L. Tsay, C. Y. Wang, J. D. Chen, and F. Y. Lin, "Generations of chaos-modulated pulses based on a gain-switched semiconductor laser subject to delay-synchronized optical feedback for pulsed chaos lidar applications," Opt. Express **28**(16), 24037–24046 (2020).
31. D. Z. Zhong, N. Zeng, H. Yang, and Z. Xu, "Precise ranging for the multi regions of two complex-shape targets by using two chaotic polarization components in the optically pumped spin vertical cavity surface emitting laser with optical injection," Acta Phys. Sin. **70**(7), 074206 (2021).
32. J. D. Chen, H. L. Ho, H. L. Tsay, Y. L. Lee, C. A. Yang, K. W. Wu, J. L. Sun, D. J. Tsai, and F. Y. Lin, "3D chaos lidar system with a pulsed master oscillator power amplifier scheme," Opt. Express **29**(17), 27871–27881 (2021).
33. C. H. Cheng, Y. C. Chen, and F. Y. Lin, "Generation of uncorrelated multichannel chaos by electrical heterodyning for multiple-input–multiple-output chaos radar application," IEEE Photon Journal **8**(1), 7800209 (2016).
34. R. Hegger, M. J. Bünner, H. Kantz, and A. Giaquinta, "Identifying and modeling delay feedback systems," Phys. Rev. Lett. **81**(3), 558–561 (1998).
35. S. Y. Xiang, W. Pan, B. Luo, L. S. Yan, X. H. Zou, N. N. Li, and H. N. Zhu, "Wideband unpredictability-enhanced chaotic semiconductor lasers with dual-chaotic optical injections," IEEE J. Quantum Electron. **48**(8), 1069–1076 (2012).
36. F. Y. Lin and J. M. Liu, "Nonlinear dynamical characteristics of an optically-injected semiconductor laser subject to optoelectronic feedback," Opt. Commun. **221**(1-3), 173–180 (2003).
37. A. K. Zhao, N. Jiang, S. Q. Liu, C. P. Xue, J. M. Tang, and K. Qiu, "Wideband complex-enhanced chaos generation using a semiconductor laser subject to delay-interfered self-phase-modulated feedback," Opt. Express **27**(9), 12336–12348 (2019).